Key Engineering Materials
ISSN: 1662-9795, Vol. 926, pp 1379-1386
doi:10.4028/p-fxk5d9

Submitted: 2022-01-17
Revised: 2022-01-18
Accepted: 2022-02-18
Online: 2022-07-22

Post-Forming Limits of Carbon Fibre Reinforced Thermoplastic Tubular Structures in a Rotary Draw Bending Process

Mengyuan Li[1,a*], Chris Stokes-Griffin[1,b], Silvano Sommacal[1,c] and Paul Compston[1,d]

[11]ARC Training Centre for Automated Manufacture of Advanced Composites, Australian National University, Canberra, ACT 2600, Australia

[a]mengyuan.li@anu.edu.au, [b]chris.stokes-griffin@anu.edu.au, [c]silvano.sommacal@anu.edu.au, [d]paul.compston@anu.edu.au

Keywords: CF/PA6; thermoplastic composite tube; post-forming; rotary draw bending; micro-CT analysis

Abstract. This paper presents the post-forming limits of polyamide 6 carbon (CF/PA6) thermoplastic tubes to facilitate design and process optimisation of bent tubular CF/PA6 part manufacturing. Straight CF/PA6 tubes can be post-formed using rotary draw bending at elevated temperature to achieve desired curvatures. Forming limits of the tubes are predicted based on their winding angles, tube geometry, and bending radius, presented as the relation between tube winding angle and bending ratio. Additionally, the corresponding principal shear strain limits are derived from the winding angle limits and tube axial strains. Three sets of CF/PA6 tubes with the configurations of $[\pm 30°]_4$, $[\pm 45°]_4$, and $[\pm 60°]_4$ are heated to 220℃ and post-formed to a bending angle of 90° with a bending ratio of 2. Micro computed tomography imaging is performed to analyse tube geometry after forming to identify forming and failure modes for tubes beyond the forming limits.

1. Introduction

The demand for composite materials has been growing over the past decades, especially in the automotive industry for the pursue of lightweight and high performance applications [1]. Carbon fibre reinforced thermoplastic tubes are highly desirable for such applications as they offer high stiffness-to-weight ratios of composites combined with the design versatility of tubes, enabling more possibilities in the making of structural components [2,3]. Currently, straight tubes can be rapidly manufactured by laser assisted thermoplastic automated tape placement (TP-ATP) [4]. The use of thermoplastic polymer matrix system opens the possibility of rapid production and customisation of carbon reinforced composite parts. Fibre relocation and re-orientation are possible via re-heating of the matrix system into a soft and formable state [5]. Therefore, formation of complex curvatures from straight thermoplastic tubes is possible via post-forming operations such as rotary draw bending (RDB) akin to metallic tubing [6].

As a post-forming technique, RDB at elevated temperature is relatively simple with notable advantages including high design freedom, reduced instrument cost, and the possibility of automation [7]. In a thermoplastic composite RDB process, it is possible for the tube undergo forming when the temperature in the bending zone is sufficiently high for significant matrix softening. In this study, a straight tube is first fed into the RDB setup, and the whole assembly is heated to the formable temperature of the tube [6,8]. The heated tube is then bent to the desired curvature defined by a bending angle under isothermal conditions [6,8]. To enable prediction of tube deformation, laminate changes, and the related mechanical property changes for design optimisation, it is important to understand the forming limits of tubes, which can be defined by tube winding angle and bending ratio between the bending radius and tube diameter.

This study will investigate the relation between CF/PA6 tube winding angles and their influence on the post-forming behaviour in a RDB post-forming process. Three sets of CF/PA6 tubes, namely $[\pm 30°]_4$, $[\pm 45°]_4$, and $[\pm 60°]_4$ will be post-formed under isothermal conditions to a bending angle of 90°. Micro computed tomography (micro-CT) will be conducted on the post-formed tubes to

analyse the geometrical changes and to identify the change of forming modes. A forming limit diagram on tube winding angle and bending ratio based on the parameters used in this study, validated by the forming experiments will be presented by this study. Based on the validated forming limits, the corresponding principal shear strains are derived and compared against the tube axial strains.

2. Post-Forming Experiments

2.1 Experimental Materials and Setup

Straight CF/PA6 tubes were manufactured at AFPT GmbH via TP-ATP using Celanese Celstran® CFR-TP PA6 CF60-01 tapes. Each tape is 12 mm wide, 0.13 mm thick, and has a fibre volume content of 48%. The tape placement rate was 12 m/min with a consolidation force of 200 N at a process temperature of 280 ℃. The tapes were wound around a chrome steel bar with the diameter of 20 mm, following a conventional helical filament winding pattern, with a shaft parameter of one ($N_s = 1$) defined by [9], and 5, 4 and 3 circuits (P) per $\pm 30°$, $\pm 45°$, and $\pm 60°$ layer pair respectively. The manufactured tubes were measured with an average tape width of 12.5mm, inner diameter (d_i) of 20 mm, and outer diameter (d_o) of 22.6 mm and had 8 plies, resulting in an average wall thickness of 1.3 mm. The winding angle of the ith ply, $\theta_{0,i}$ is computed based on the tube ply circumference, $2\pi r_i$, the tape width, w, and P.

$$\theta_{0,i} = \cos^{-1}\left(\frac{wP}{2\pi r_i}\right) \quad (1)$$

A bespoke rotary draw bender was manufactured for the post-forming experiments. The bender contains key elements akin to a traditional metal tube bender with modifications including the polytetrafluoroethylene (PTFE) pressure and wiper dies to minimise heat loss during forming, and the addition of a bending angle selector for curvature setting and a silicone mandrel for internal support. The main bending die has a mid-line bending radius of 46mm, making the bending ratio 2.

2.2 Experimental Procedure

Post-forming of CF/PA6 tubes requires heating of the tubes to their formable temperature of 220℃ to soften the thermoplastic matrix prior to forming [6,8]. In this post-forming experiment, a silicone mandrel with its diameter equivalent to d_i and length greater than the tube bending zone length, was inserted into the tube. An Omega 5SC-TT-K-40-36 fine wire K-type thermocouple was inserted between the mandrel and the tube bending zone to monitor temperature change in the experiment. A National Instruments cDAQ-9188 data logger was used to record the temperature data readings.

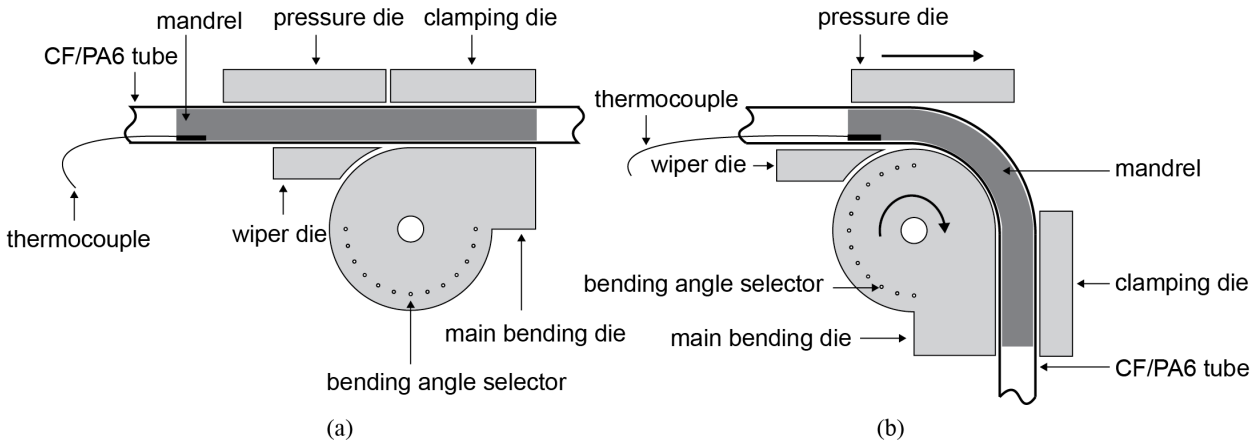

Figure 1 RDB operation for CF/PA6 tubes (a) tube loading and heating, (b) tube bending and clamping

The tube was then loaded into the bender, which was heated until the thermocouple read 220℃ in a Steridium O75 Oven. The duration of heating phase was approximately five hours per tube. The loaded tube was bent by turning the main bending die to 90° at a bending rate of approximately 45°

per second and held in place until tube temperature dropped below 100℃. This allowed for the re-solidification of the thermoplastic matrix while the bent tube was constrained at the desired geometry to minimise spring-back [6].

3. Post-Forming Tube Characterisation

Using micro-CT imaging of the post-formed CF/PA6 tubes, tube diameter, d, and tube bending zone length, l are characterised to determine tube axial strain, ε_x and ovality changes during forming to identify possible changes in forming modes for tubes with varying θ_0. ε_x is formulated based on the characterised bending zone length before (l_0) and after (l_1) forming.

$$\varepsilon_x = \frac{l_1 - l_0}{l_o} \tag{2}$$

The post-formed tubes were imaged using a HeliScan™ micro-CT instrument at the Australian National University (ANU) CTLab. The instrument was equipped with a 60kV X-ray micro-focus source and a 3040 x 3040 pixels flat panel detector. 2D radioscope projections were taken of individual specimens, placed on a rotating motor-controlled stage, after each rotation. Volumetric images of the complete 3D post-formed CF/PA6 tube geometry were obtained from the processing of the 2D projections using a proprietary ANU reconstruction algorithm [10]. Total acquisition time was ~17 hours, total number of projections was 8778, and scanning resolution (i.e. voxel size) was ~45 µm for the tubes bent to 90°.

4. Forming Limit Model

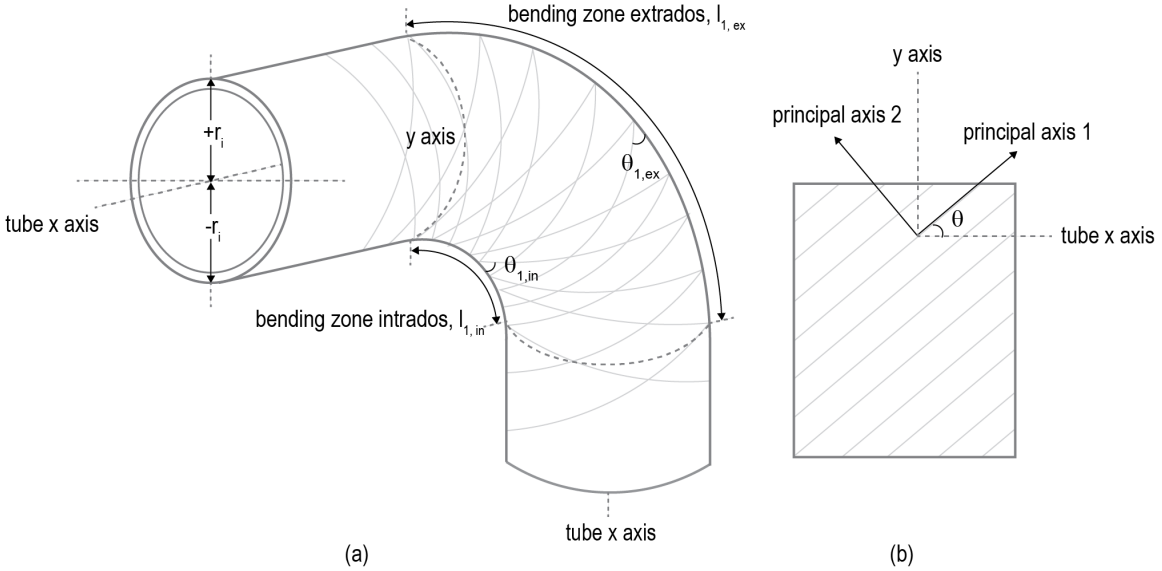

Figure 2 (a) Parameters of a post-formed CF/PA6 tube, (b) laminate off-axis coordinates

CF/PA6 tube post-forming limits can be expressed in terms of its winding angle limits corresponding to a given bending ratio based on the post-forming fibre orientation prediction model by Eckardt et al [8]. The fibre orientation prediction model predicts the ultimate fibre angle, θ_1 (maximum and minimum) in a post-formed tube based on the initial fibre angle, θ_0 and the bending radius, r_b and tube ply radius, r_i. The model assumes a pure textile tube deformation during forming, in which only rotational displacement of the crossing tapes at their points of intersection is possible according to [8]. In the formulation of θ_1, fibre lengths are assumed to be constant due to their high stiffness relative to the molten thermoplastic matrix and the tube circular cross section represented by r_i is also assumed to be constant. Additionally, the model neglects slipping effects, resulting in a constant distance between two intersection points [8]. After forming, the maximum and minimum

fibre angles can be found at the intrados and the extrados respectively, where the maximum axial strains are experienced by the tube during forming.

$$\theta_{1,ex} = \cos^{-1}\left(\frac{r_b+r_i}{r_b}\cos\theta_0\right) \quad (3)$$

$$\theta_{1,in} = \cos^{-1}\left(\frac{r_b-r_i}{r_b}\cos\theta_0\right) \quad (4)$$

5. Results and Discussion

5.1 CF/PA6 Tube Winding Angle Limits

During forming, the extrados experiences a tensile strain and elongates while the intrados experiences a compressive strain and compresses. Consequentially, the extrados fibres align towards the axial direction ($\theta = 0$) parallel to the tube axis due to the axial tension and the intrados fibres align towards the hoop direction ($\theta = 90°$) normal to the tube axis due to the axial compression. As the fibres are wound between the axial and hoop directions and cannot completely align with the axes, $\theta_{1,ex} > 0$ and $\theta_{1,in} < 90°$. Hence, the limits of θ_0 can be derived to satisfy these conditions based on Eq. (3) and (4).

$$\theta_0 > \cos^{-1}\left(\frac{r_b}{r_b+r_i}\right) \quad (5)$$

$$\theta_0 < (\cos^{-1} 0 = 90°) \quad (6)$$

The limits of θ_0 of a given set of bending parameters can be obtained by substituting the parameters into Eq. (5) and (6). The lower limit of θ_0 from Eq. (5) is valid when $r_i \neq r_b$ and $r_i < r_b$, suggesting that θ_0 is inversely proportional to the bending ratio. The upper limit from Eq. (6), on the other hand, is always satisfied with fibres oriented between the axial and hoop directions. Based on the parameters used in the forming experiments, the lower limit is valid in this study and are computed to compare with θ_0 of each laminate configuration of the experimental CF/PA6 tubes in Table 1. A $\pm 2°$ variation was observed from the measured θ_0 of the tube outer plies in the experiment.

Table 1 Comparison of the limits and actual $\theta_{0,i}$ of $[\pm\theta_0]_4$ CF/PA6 tubes

Ply	1	2	3	4	5	6	7	8
Diameter [mm]	20	20.325	20.65	20.975	21.3	21.625	21.95	22.275
Upper limit (intrados) $\theta_{0,in}$ [°]	90	90	90	90	90	90	90	90
$[\pm 60°]_4$ [°]	53.36	54.04	54.69	55.31	55.92	56.50	57.06	57.60
$[\pm 45°]_4$ [°]	37.27	38.46	39.58	40.64	41.65	42.61	43.53	44.40
$[\pm 30°]_4$ [°]	5.89	11.82	15.55	18.47	20.93	23.08	24.99	26.73
Lower limit (extrados) $\theta_{0,ex}$ [°]	34.82	35.02	35.21	35.51	35.71	35.90	36.20	36.39

The lower limit of θ_0 derived from the prediction model is 34.82° for ply 1, which corresponds to that of the $[\pm 45°]_4$ laminate configuration. From Fig. 3, buckling is observed on the intrados of the $[\pm 30°]_4$ and $[\pm 45°]_4$ tubes after forming while the intrados of the $[\pm 60°]_4$ tube follows the design curvature with no visible failure. In this case, failure to post-form the $[\pm 30°]_4$ and $[\pm 45°]_4$ tubes due to buckling agrees with the lower formable limit of $[\pm 45°]_4$ from model derivation.

5.2 CF/PA6 Tube Post-Forming Mode Change

Eq. (3) and (4) predict that tubes with smaller θ_0 experience larger fibre angle change during forming. For tubes with θ_0 smaller than the lower limit, axial strain during forming acts predominantly in the fibre direction. In this case, when the required fibre angle change is greater than θ_0, the forming mode changes from fibre realignment reflected by the smooth surface finish of the

formed $[\pm 60°]_4$ tube with no visible failures into fibre buckling as observed on the formed $[\pm 30°]_4$ and $[\pm 45°]_4$ tubes in Fig. 3. At tube intrados, compression of axially-aligned fibres in the axial direction forces fibres to buckle rather than to realign. At tube extrados, as the fibres realign to the axial direction due to tension to form the elongated extrados, inward displacement of extrados towards the bending die may occur as a result of the realigned fibres being unable to span the full length of the extrados.

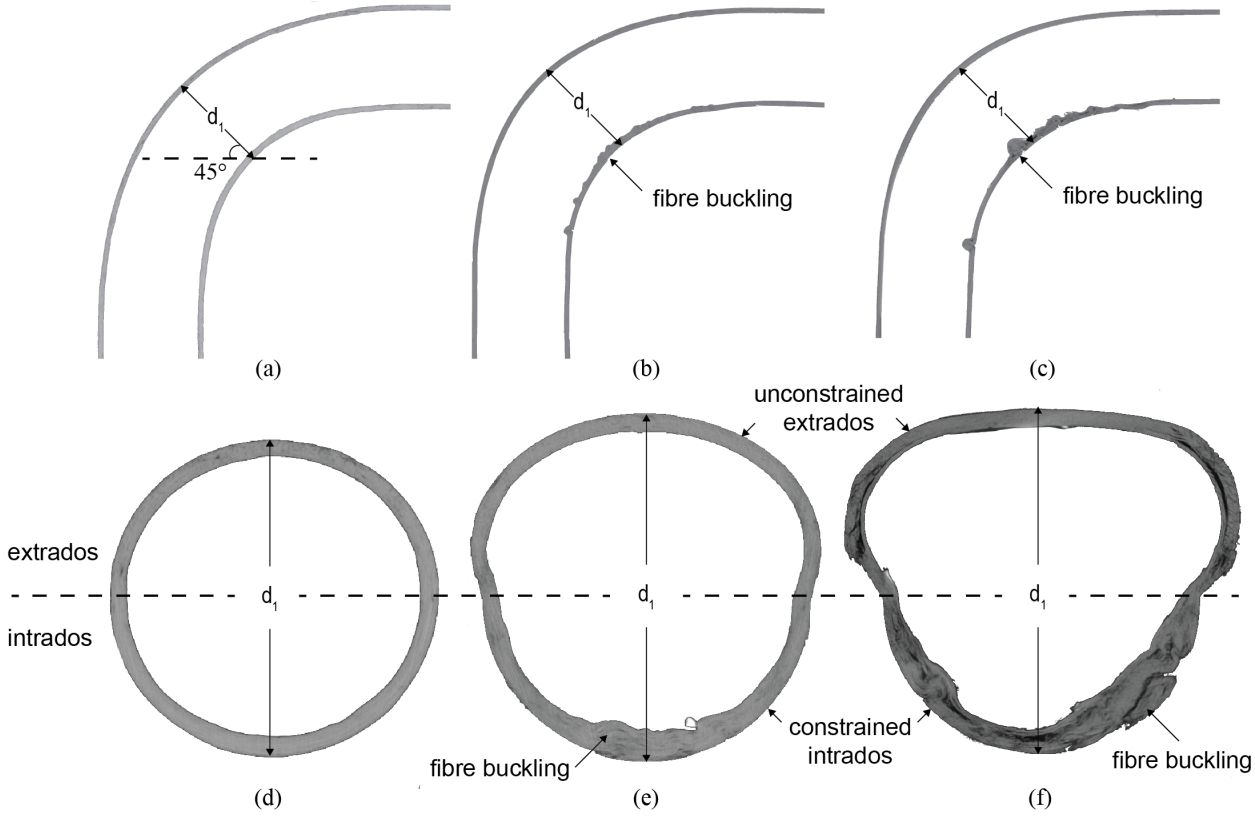

Figure 3 Micro-CT mid-plane cross-section image of (a) $[\pm 60°]_4$*, (b)* $[\pm 45°]_4$*, and (c)* $[\pm 30°]_4$ *CF/PA6 tubes and bend centre (angular position = 45°) circumferential cross-section image of (d)* $[\pm 60°]_4$*, (e)* $[\pm 45°]_4$*, and (f)* $[\pm 30°]_4$ *CF/PA6 tubes*

From the circumferential cross-section of the tubes taken at the angular position of 45°, deformation is found at the extrados of the formed $[\pm 30°]_4$ and $[\pm 45°]_4$ tubes. d_1 measured vertically from the outermost ply increases significantly by an average of 14.51% and 8.10% after forming for the $[\pm 30°]_4$ and $[\pm 45°]_4$ tubes respectively. d_1 of the $[\pm 60°]_4$ tubes, on the other hand, experienced a slight decrease after forming by an average of 5.88%. The reduction of d_1 in tubes within the forming limits reflects the inward displacement of the extrados due to the tensioning of fibres. For the tubes beyond the forming limits, the inward extrados displacement were accompanied by horizontal expansions of the extrados half of the tubes as well as elongated d_1. As the tube intrados was constrained by the main bending die, the outer wall of the intrados maintained the desired curvature and ovality of the tube.

The extrados deformation of the tubes beyond the forming limits may be caused by the joint effect of both the intrados and extrados under the forming strains. Buckling was induced at the intrados due to compressive strain. The thickened intrados wall due to buckling pushed the silicone mandrel against the extrados, forcing the extrados to expand, hence resulting in elongated d_1. On the other hand, tensile strain experienced by the extrados resulted in its inward displacement as it could not be stretched to cover the increased extrados length after forming, hence forming the flattened extrados surface. The extrados surface was flattened more in tubes with smaller θ_0 as the extrados fibres were more axially aligned. As the tube extrados was not constrained, the compression by its inward displacement induced horizontal expansions on the unconstrained sides.

5.3 CF/PA6 Tube Forming Limits

With the validated forming limit derivation by the experimental results, the forming limit diagram of the CF/PA6 tubes in terms of the minimum θ_0 required for a given bending ratio based on the parameters used in this study is established. In the forming limit diagram (Fig. 4), diameter of the ply is set as 20 mm, the diameter of ply 1, as it has the lowest winding angle, and tape width as 12.5 mm. The bending ratios range from 1 to 20 by adjusting r_b while keeping other parameters consistent. From Fig. 4, the minimum winding angle shows an exponential decrease as bending ratio increases.

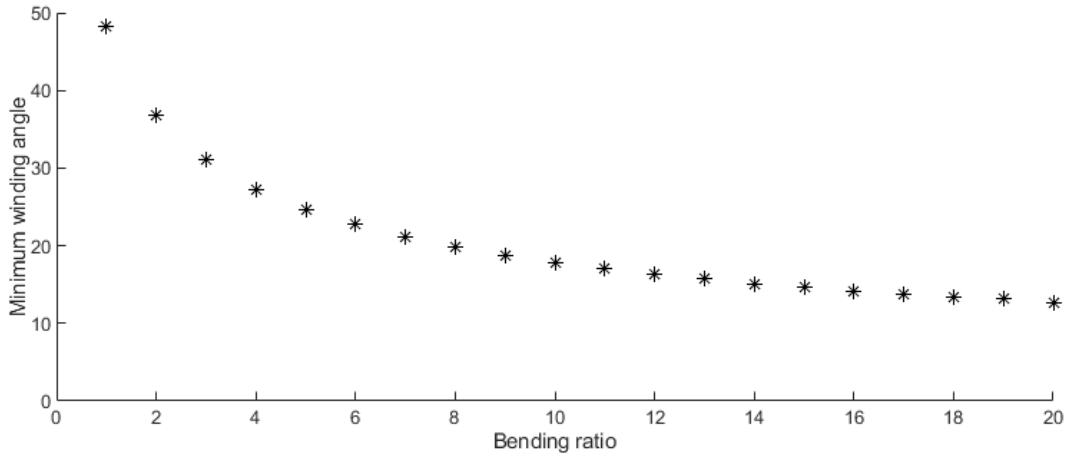

Figure 4 Forming limit of CF/PA6 tubes: minimum θ_0 with respect to tube bending ratio

5.4 CF/PA6 Tube Post-Forming Strain Limits

In terms of fibre shear during forming, the shear strains experienced by the tapes and the tube can be related by a transformation matrix [T] based on the sine (s) and cosine (c) operations of θ_0. The x and y axes of the tube correspond to its axial and hoop directions respectively as shown in Fig. 2. The tube normal strains, ε and the shear strain, γ on the x and y axes are transformed into principal material coordinates, corresponding to the axial and transverse fibre orientations of the tape.

$$\begin{Bmatrix} \varepsilon_1 \\ \varepsilon_2 \\ \gamma_{12}/2 \end{Bmatrix} = \begin{bmatrix} c^2 & s^2 & 2cs \\ s^2 & c^2 & -2cs \\ -cs & cs & c^2 - s^2 \end{bmatrix} \begin{Bmatrix} \varepsilon_x \\ \varepsilon_y \\ \gamma_{xy}/2 \end{Bmatrix} = [T] \begin{Bmatrix} \varepsilon_x \\ \varepsilon_y \\ \gamma_{xy}/2 \end{Bmatrix} \tag{7}$$

As the fibre angle prediction model assumes a constant r_i, no hoop strain is experienced by the tube during forming, which is reflected by $\varepsilon_y = 0$ in Eq. (7). In addition, fibres are assumed to be non-stretchable, hence $\varepsilon_1 = 0$ in Eq. (7) for fibres under tension at the extrados. It is worth noting that ε_1 may become negative at the intrados due to buckling of fibres under compression.

$$\gamma_{12} = -\frac{c}{s}\varepsilon_x \tag{8}$$

Based on the above assumptions and the known parameters, shear strain experienced by the fibres, γ_{12} at the extrados can be derived using Eq. (8) based on ε_x calculated in Eq. (2). The factor $-\frac{c}{s}$ suggests that a greater shear is experienced by the fibres with smaller θ_0 at the extrados, resulting in greater fibre angle change from smaller θ_0 predicted by Eq. (3) and (4).

Due to the cross-winding pattern of the tubes, the magnitude of shear strain limit, $|\gamma_{12,max}|$ for the extrados is compared with the extrados axial strain, $\varepsilon_{x,extrados}$ in Fig. 5. $|\gamma_{12,max}|$ is derived based on the limits of θ_0 from Fig. 4 and $\varepsilon_{x,extrados}$. The fibre angle prediction model assumptions may become invalid when beyond the principal shear strain limits of $|\gamma_{12,max}| < |\gamma_{12}| < 0$, resulting in the mode of tube post-forming to change from fibre relocation and reorientation to fibre buckling in the context of this study.

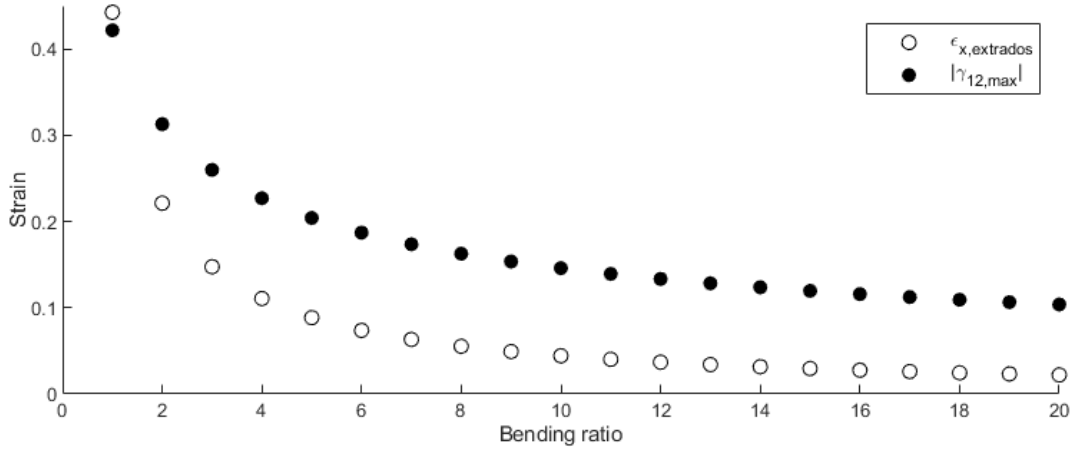

Figure 5 Comparison of tube extrados axial strains and extrados principal shear strains

From Fig. 5, both strains decrease as bending ratio increases. Between the strains, $|\gamma_{12,max}|$ has a larger magnitude than $\varepsilon_{x,extrados}$ at bending ratio ≥ 2, where the minimum $\theta_0 < 45°$; $|\gamma_{12,max}| < \varepsilon_{x,extrados}$ at bending ratio 1 when the minimum $\theta_0 > 45°$. For the bending ratio of 2 used in this study, the minimum θ_0 of 34.815° translates to the maximum γ_{12} of -0.313.

6. Conclusion

In this study, the forming limits of CF/PA6 tubes are presented in terms of a forming limit diagram and the corresponding strains to facilitate design and process optimisation of CF/PA6 component manufacturing. CF/PA6 tube forming limits are derived in terms of their winding angle limits based on a given rotary draw bending ratio from the fibre orientation prediction model and are independent of tube bending angle. Forming experiments were conducted to post-form $[\pm 30°]_4$, $[\pm 45°]_4$, and $[\pm 60°]_4$ tubes into the bending angle of 90° at 220℃ under isothermal conditions with a bending ratio of 2. Failure to form the $[\pm 30°]_4$ and $[\pm 45°]_4$ tubes agreed with the derived winding angle lower limit of $[\pm 45°]_4$.

Analysis of micro-CT images revealed that when θ_0 exceeds the limits, forming mode changes from fibre realignment and reorientation to fibre buckling through the following failures captured:

- Buckling at the intrados due to compressive strains;
- Elongated tube circumferential cross section due the silicone mandrel displaced by the buckled intrados wall;
- Flattened extrados wall as a result of its inward displacement as the extrados fibres cannot be stretched to cover the increased extrados length; and
- Horizontal expansions on the extrados side walls due to compression of the silicone mandrel induced by the inward displacement of the extrados.

Using a general orthotropic off-axis strain transformation, the shear strains experienced by the tapes can be determined based on tube strains. The magnitude of extrados principal shear strains decreases towards 0 as the bending ratio increases and they surpass the extrados tube axial strain when the bending ratio is greater than 2.

Future work will include further validations and improvements in the forming limit model via post-forming of CF/PA6 tubes at larger bending ratios. Additionally, experimental characterisation may be conducted to further investigate and validate the strain predictions. Slow motion capture of the forming process may also be implemented to further investigate tube geometrical changes during forming, hence the change of forming modes.

References

[1] E.C. Claunch, Forecasting on composites – markets, products, and demands, Journal of Textile and Apparel, Technology and Management. 9 (2015) 6.

[2] R.G. Tornero, Composite materials are more present today than ever before in cars, Reinforced Plastics. 59 (2015) 131.

[3] J. Osborne, Automotive composites – in touch with lighter and more flexible solutions, Metal Finishing. 111 (2013) 26–30.

[4] M. Schäkel, S.M.A. Hosseini, H. Janssen, I. Baran, C. Brecher, Temperature analysis for the laser-assisted tape winding process of multi-layered composite pipes, Procedia CIRP. 85 (2019) 171–176.

[5] M. Asim, M. Jawaid, N. Saba, Ramengmawii, M. Nasir, M.T.H. Sultan, 1 - Processing of hybrid polymer composites—a review, Hybrid Polymer Composite Materials. (2017) 1–22.

[6] B. Engel, J. Böcking, Bending of fibre-reinforced thermoplastic tubes, The 20th International Conference on Material Forming. (2015) 9.

[7] T. Banno, A. Rashidi, B. Crawford, A.S. Milani, A. Nakai, Development of bend-forming technologies on CFRTP tube, 21st International Conference on Composite Materials. (2019) 6.

[8] S. Eckardt, D. Barfuß, J. Condé-Wolter, M. Gude, V. Würfel, J. Böcking, Study on bend-forming behaviour of thermoplastic tape-braided CFRTP profiles, SAMPE European Conference. (2020) 9.

[9] J. Rousseau, D. Perreux, N. Verdière, The influence of winding patterns on the damage behaviour of filament-wound pipes, Composites Science and Technology. 59 (1999) 1439–1449.

[10] G.R. Myers, A.M. Kingston, S.J. Latham, B. Recur, T. Li, M.L. Turner, et al, Rapidly converging multigrid reconstruction of cone-beam tomographic data, SPIE Optical Engineering + Applications. 9967 (2016).